PHYSICAL REVIEW B VOLUME 32, NUMBER 8 15 OCTOBER 1985

Interactions, local order, and atomic-rearrangement kinetics in amorphous nickel-phosphorous alloys

Thomas A. Weber and Frank H. Stillinger
AT&T Bell Laboratories, Murray Hill, New Jersey 07974
(Received 23 May 1985)

Molecular-dynamics computer simulations have been carried out to study the liquid and amorphous solid states for a system comprising 120 Ni and 30 P atoms. This study utilized additive central pair potentials to model the interactions. Emphasis has been placed on the geometry of the resulting potential-energy hypersurface for the system as a whole to explain temperature dependence of short-range order, and to characterize bistable degrees of freedom that dominate low-temperature properties in this, and other, amorphous solids. A small collection of transition states and associated reaction coordinates for such degrees of freedom has been numerically constructed. The corresponding atomic motions tend to be localized mainly on a small subset of the atoms, but are diverse insofar as which chemical species are involved, in barrier height and asymmetry, and in the nonlinearity of the collective reaction coordinate.

I. INTRODUCTION

Both technological needs[1-3] and basic scientific curiosity[4] underlie the present intense study of amorphous materials. While theory has been able to supply a few key insights into atomic level mechanisms for the rich set of phenomena observed experimentally, many unanswered questions remain. The present work provides a conceptual framework that seems capable of answering many of those questions. Specific computations devoted to the amorphous nickel-phosphorous alloy system are reported below to illustrate our general method.

This paper represents an extension of an earlier report[5] also devoted to the Ni-P system. As noted in that predecessor, our initial estimate of the atomic pair interactions was somewhat deficient, and an improved version was proposed. The present study utilizes that improved set of interactions, the details of which are contained in Sec. II.

The novel features of this and recent related work[5-13] on the classical many-body problem stem from careful examination of the differential geometry of the potential energy hypersurface. In particular this concerns the local minima, their distribution by depth, and the nature of the saddle-point regions separating neighboring pairs of minima. The topography of this hypersurface in the multidimensional configuration space for a many-body system obviously controls the dynamical trajectories available to that system. Those trajectories in turn determine kinetic properties as well as equilibrium structure.

Section II briefly outlines our Ni-P model and how it has been investigated at the near-eutectic composition of 80 at. % Ni + 20 at. % P by means of molecular dynamics simulation. During the course of many of our molecular dynamics runs we have implemented a mapping of instantaneous system configurations onto nearby potential-energy minima (without however disturbing the conservative dynamics). This mapping is generated by a mass-weighted steepest descent on the potential-energy hypersurface, and creates a running record of the stable atomic packings (potential minima) within whose ambits the dynamics carries the system as time proceeds.

Section III presents some results concerning short-range order in the Ni-P alloy. In particular we have evaluated the three independent pair-correlation functions g_{NiNi}, g_{NiP}, and g_{PP} under conditions of thermal equilibrium, but over a wide temperature range. In line with conventional expectations, temperature increase causes the degree of short-range order revealed by these functions to decrease substantially. The sets of system configurations contributing to the above pair-correlation functions also have been mapped onto potential-energy minima, and the results utilized to compute sets of "quenched pair-correlation functions" $g_{\mathrm{NiNi},q}$, $g_{\mathrm{NiP},q}$, and $g_{\mathrm{PP},q}$. Not only does this mapping produce substantial "image enhancement" of the short-range order, but it also demonstrates (under fixed density conditions) that this enhanced short-range order is independent of starting temperature (if it is above the glass transition), and thus it is an inherent structural attribute of the liquid phase. This latter property seems to have applicability that extends well beyond the Ni-P alloy system, and certainly encompasses monatomic model substances which easily crystallize.[6,8-13]

Section IV examines the statistical topography of the potential hypersurface for the Ni-P alloy by means of two further numerical probes. The first concerns mean atom return distances under operation of the mapping to minima. The second involves the distribution of eigenvalues for the Hessian matrix of second derivatives of the potential function. Both illustrate the high degree of anharmonicity involved in those regions of configuration space that typically contribute to the solid even below its glass temperature, and even more so to the liquid phase.

The delicate numerical problems associated with locating and characterizing transition states (saddle points) receive attention in Sec. V. Despite difficulties, a group of such transition states and their associated collective reac-

tion coordinates have been constructed. These results provide a very detailed picture of the way that bistable degrees of freedom can create "two-level systems" that apparently dominate low-temperature heat capacity, thermal expansion, and phonon scattering in many low-temperature amorphous solids.[14,15]

The final section (Sec. VI) discusses further possible areas of application for the multidimensional geometric approach followed herein.

II. MODEL AND SIMULATION DETAIL

For a wide range of materials such as noble gases,[6,8,9] alkali metals,[11,12] binary mixtures,[5] and bulk silicon,[13] appropriate effective pair interactions have been found to be well represented by a family of functions of the form

$$v(r)=\begin{cases} A\,[(\alpha r)^{-p}-(\alpha r)^{-q}]\exp[(\alpha r-a)^{-1}], & 0<\alpha r\le a \\ 0, & \alpha r\ge a \end{cases} \tag{2.1}$$

where A, α, P, and a are strictly positive. This functional form is particularly useful in simulation studies because its range of interaction is limited, and it is continuous and all its derivatives exist for positive r. In addition the parameters provide sufficient flexibility so that using only these pair interactions for pure substance applications either the fcc or bcc lattices can have the lowest energy at zero temperature and pressure.

This potential form was also found[5] to represent adequately the metal-metal, metal-metalloid, and metalloid-metalloid pair interactions in the Ni-P binary alloy system. The total potential energy may be written for such a system as

$$\Phi(\mathbf{r}_1,\mathbf{r}_2,\ldots,\mathbf{r}_N)=\sum_{\substack{i,j=1\\ i<j}}^{N} v_{\kappa(i)\kappa(j)}(r_{ij}) \tag{2.2}$$

where $\kappa(i)$=Ni or P indicating the species of atom i. It is convenient to choose reduced units for Φ so that the metal-metal pair interactions have unit depth at the minimum and are zero at $r=1$. The following parameter choices were found to reproduce adequately the important features of the amorphous Ni-P alloy in comparison with experimental x-ray scattering data:[16] (a) For all interactions,

$$p=12,\quad q=0,\quad a=1.652\,194\,. \tag{2.3}$$

(b) For the metal-metal interaction v_{NiNi},

$$A=1.0\times 8.805\,977,\quad \alpha=1.0\,. \tag{2.4}$$

(c) For the metal-metalloid interaction v_{NiP},

$$A=1.5\times 8.805\,977,\quad \alpha=2.49/2.20=1.1318\ldots\,. \tag{2.5}$$

(d) For the metalloid-metalloid interaction v_{PP},

$$A=0.5\times 8.805\,977,\quad \alpha=2.49/2.20=1.1318\ldots\,. \tag{2.6}$$

This choice of parameters yields the correct crystal structure (fcc) for the pure Ni and also assures that the bond lengths for the pure Ni and pure P are in the correct ratio (2.49 Å to 2.20 Å).

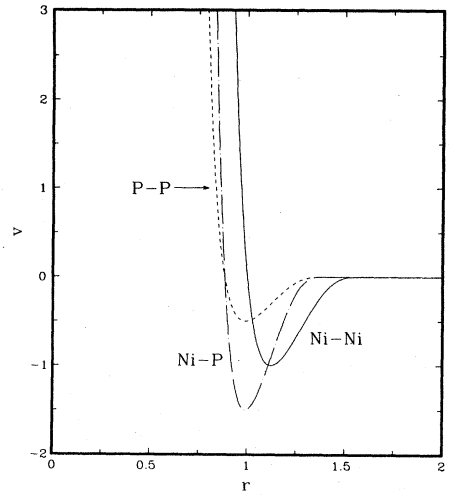

FIG. 1. Pair interaction potentials (in units of ϵ, the metal-metal interaction energy) as a function of the interatomic separation distance (in units of σ, the metal-metal characteristic separation distance).

Figure 1 shows a plot of the three pair interaction potentials as a function of separation distance. The relative depths at the potential minima are 1.0, 1.5, and 0.5 for the Ni-Ni, Ni-P, and P-P pair interactions respectively, and agree roughly with the expected relative bond strengths.

The molecular dynamics simulations were carried out with 150 atoms: 120 Ni atoms and 30 P atoms. This alloy mixture is close in composition to the deep eutectic found at 19.11 at. % P. The stable isotopes ^{62}Ni and ^{31}P were used in the simulations, corresponding to reduced masses 1.0 and 0.5, respectively.

The Newtonian equations of motion

$$m_i\frac{d^2\mathbf{r}_i}{dt^2}=-\nabla_i\Phi\,, \tag{2.7}$$

where m_i is the mass of the ith atom, were solved using a fifth-order Gear algorithm,[17] and reduced time step $\Delta t=5\times 10^{-4}$. Classical dynamical trajectories of 10^4 time steps were generated to determine average thermodynamic properties of the alloy. Temperature changes were implemented by the usual momentum scaling, followed by relaxation runs of 2×10^3 steps which were discarded before averages were accumulated.

During the course of generation of a dynamical trajectory, configurations of the 150 atoms were sampled (typically every 100 time steps) and subjected to a "quenching" procedure to determine the instantaneously relevant structurally stable packings (Φ minima). This quenching involved a mass-weighted steepest descent that requires solving

$$m_i\frac{\partial\mathbf{r}_i}{\partial s}=-\nabla_i\Phi\,, \tag{2.8}$$

with the given system configuration serving as initial con-

ditions. The $s \to +\infty$ solutions to Eq. (2.8) were constructed using a Newton's method.[18] The quench procedure does not affect the course of the subsequent dynamical trajectory generation, but is simply carried out as an independent, informative monitoring device.

In order to compare the simulation results with measurements it is necessary to redimension the simulation data. The unit of mass is that of the ^{62}Ni atom:

$$m_{\mathrm{Ni}} = 1.0284 \times 10^{-22} \text{ g} . \tag{2.9}$$

The unit of length is

$$\sigma = 2.2183 \text{ Å} \tag{2.10}$$

which places the Ni-Ni pair potential minimum at 2.49 Å. The energy scale is

$$\epsilon = 1.8546 \text{ kcal/mol} = 1.2879 \times 10^{-13} \text{ erg/atom} , \tag{2.11}$$

which causes the melting point of the pure metal measured from simulation at 1.85 reduced units[8] to agree with the measured melting temperature for Ni, 1453 °C. The eutectic temperature T_{eu}, equal to 880 °C, corresponds to reduced temperature 1.2358. The simulations were performed at constant mass density 8.348 g/cm^3, chosen so that the number density agreed with experiment (we use ^{62}Ni and ^{31}P rather than the naturally occurring mixtures of isotopes, so our mass density is higher than that normally found in experiments).

The fundamental unit of time is therefore

$$\tau = \sigma(m_{\mathrm{Ni}}/\epsilon)^{1/2} = 6.2721 \times 10^{-13} \text{ s} . \tag{2.12}$$

Each molecular dynamics run of 10^4 steps consequently spans $5\tau = 3.1361$ ps.

III. INHERENT STRUCTURES

Figure 2 shows a plot of average potential energy per atom, ϕ, as a function of temperature (both in reduced units). Each point is an average over a 3.1361-ps run, and the points were generated during both heating and cooling cycles.

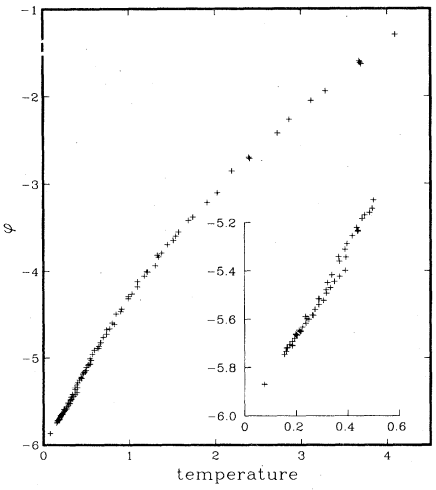

FIG. 2. Average potential energy per atom for the Ni-P alloy as a function of temperature, both in reduced units.

The inset in Fig. 2 shows the scatter in the data at low temperatures which results from the different thermal histories of the low-temperature samples. All of these low-temperature solids correspond to amorphous packings of Ni and P atoms; no crystalline structures were ever discovered in the course of the coolings.

Fundamental information about atomic arrangements in the Ni-P alloy resides in the three radial pair-correlation functions g_{NiNi}, g_{NiP}, and g_{PP}. These functions are defined by requiring that the probability that two volume elements dV_1 and dV_2 separated by distance R_{12} will respectively be occupied by species μ and κ (Ni or P) is

$$\rho_\mu \rho_\kappa g_{\mu\kappa}(R_{12}) dV_1 dV_2 , \tag{3.1}$$

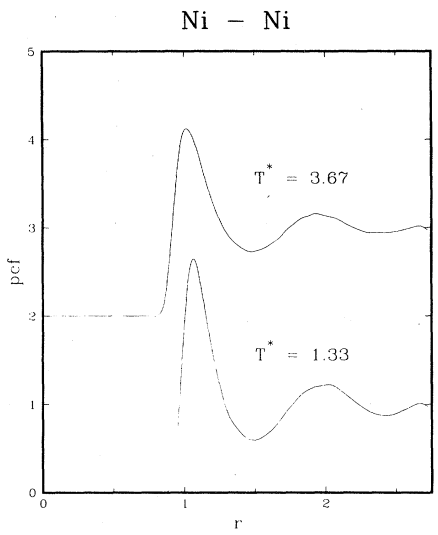

FIG. 3. Metal-metal pair-correlation functions. The zero of the high-temperature case has been offset.

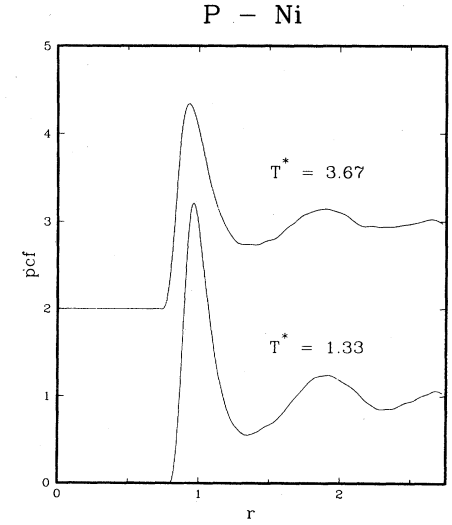

FIG. 4. Metal-metalloid pair-correlation functions.

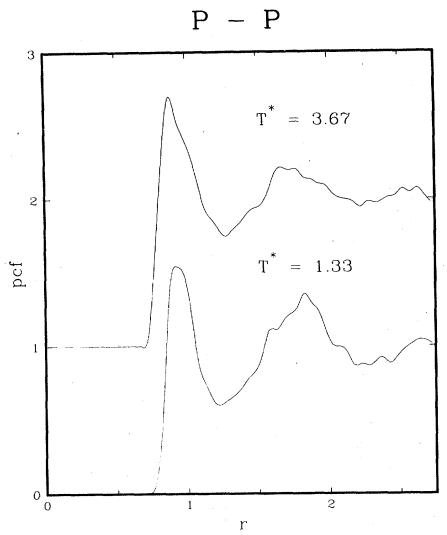

FIG. 5. Metalloid-metalloid pair-correlation functions.

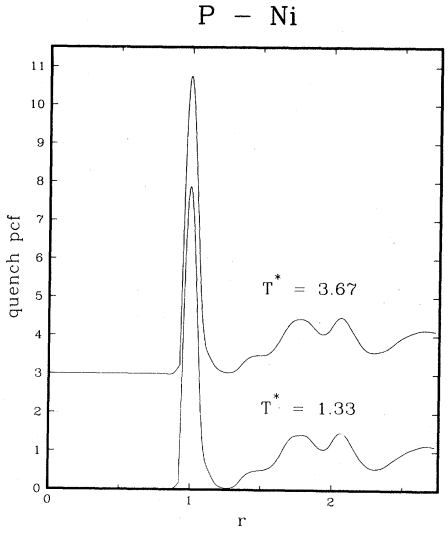

FIG. 7. Metal-metalloid pair-correlation functions determined from the quenched configurations. The curves correspond to the same thermodynamic states shown in Fig. 4.

where ρ_μ and ρ_κ are the number densities. The normalization is such that in an infinite system

$$\lim_{R_{12}\to\infty} g_{\mu\kappa}(R_{12})\to 1 \ . \tag{3.2}$$

Figures 3—5 show our results for these three pair-correlation functions at two temperatures, one near the eutectic temperature and the other at a much higher temperature. The two reduced temperatures are 1.33 and 3.67, and correspond respectively to 968 °C and 3151 °C.

The results show that raising the temperature decreases the short-range order, as expected. The curves in Fig. 5 for g_{PP} are subject to considerable statistical "noise" due to the small number of P atoms present. Nevertheless, it is obvious that the pairs of P atoms are relatively uncorrelated at both temperatures, in comparison to the other two types of atom pairs present in the system.

Figures 6—8 show quench pair-correlation functions $g_{\mu\kappa,q}$ calculated from the same thermodynamic states involved in Figs. 3—5. These functions were generated by constructing pair-correlation functions from the quench configurations that were determined every 0.031 361 ps along the trajectory and then averaging these 101 configurations to produce the curves shown.

It is clear from the figures that the "quench" pair-correlation functions are substantially independent of the temperature of the trajectories from which they are calcu-

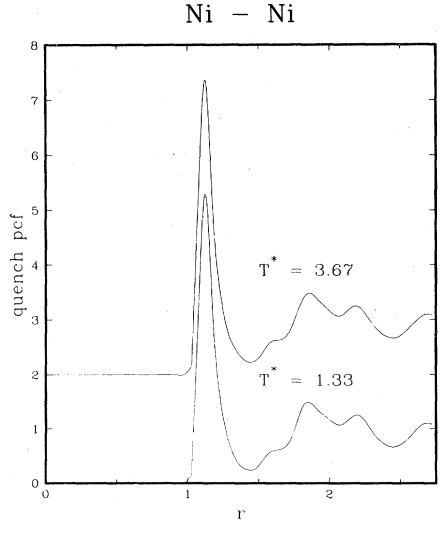

FIG. 6. Metal-metal pair-correlation functions determined from the quenched configurations. The curves correspond to the same thermodynamic states shown in Fig. 3.

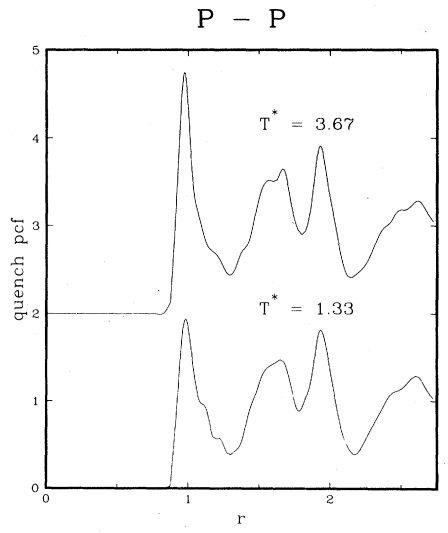

FIG. 8. Metalloid-metalloid pair-correlation functions determined from the quenched configurations. The curves correspond to the same thermodynamic states shown in Fig. 5.

lated, provided those temperatures are above the eutectic temperature T_{eu}. Although only two temperature extremes are shown, this conclusion is based also on a large number of other quench pair-correlation functions calculated at intermediate temperatures. Well below T_{eu} this temperature independence starts to break down as the system becomes locked into atypical regions of phase space. This becomes particularly noticeable at or below reduced temperature 0.4 (cf. Fig. 2).

The difference in the quench pair-correlation functions in Fig. 8 may be ascribed to a sampling problem due to the relatively small number of P atoms. The running coordination number of atoms at the first minimum of $g_{PP,q}$ at $r=1.275$ is 6.51 for $T=3.67$ and 5.51 for $T=1.33$. Note in Fig. 8 that these two curves are more nearly identical at larger distances where the number of contributing P-P pairs increases.

IV. HYPERSURFACE GEOMETRY

The geometry of the potential energy hypersurface for the Ni-P alloy may be examined and characterized by the mean atomic return distance to the quench minima, and by the principal curvatures of the hypersurface deduced from the eigenvalues of the Hessian matrix. The average mean return distance that an atom traverses in going from any point on the potential-energy hypersurface to its associated stable potential energy local minimum configuration is defined as

$$d_\mu = \left\langle \left[\sum_i (\mathbf{r}_i - \mathbf{r}_{i,q})^2 / N_\mu \right]^{1/2} \right\rangle , \tag{4.1}$$

where the summation is only over atoms of type μ (Ni or P), $\mathbf{r}_i$ is the position of the ith atom of type μ, $\mathbf{r}_{i,q}$ is its position at the quench minimum, and N_μ is the total number of atoms of type μ.

Figure 9 shows how the mean return distances for the Ni and for the P atoms vary with temperature. Each point represents an average over 101 distinct quenchings. These return distances increase rapidly with temperature up to roughly T_{eu}, but flatten considerably at higher temperature. Although results for the two species are similar there is a crossover at reduced temperature 0.8, with Ni tending to move farther at lower temperature, P at higher temperature.

In contrast to the present case, substances which crystallize exhibit a marked discontinuity in the mean return distance at the melting point, T_m. Below T_m these return distances are related to the Lindemann melting criterion, while above T_m they provide a complementary freezing criterion.[13,19]

Another illuminating probe of Φ hypersurface geometry emerges from eigenvalues of the Hessian matrix $\underline{\mathbf{K}}$. These are defined by the determinantal equation

$$|\underline{\mathbf{K}} - \omega^2 \underline{\mathbf{I}}| = 0 , \tag{4.2}$$

where $\underline{\mathbf{I}}$ is the unit matrix. The elements of $\mathbf{K}$ are given by

$$K_{i\alpha,j\gamma} = (m_i m_j)^{-1/2} \frac{\partial^2 \Phi}{\partial x_{i\alpha} \partial x_{j\gamma}} \tag{4.3}$$

where $x_{i\alpha}$ is the αth component of position vector $\mathbf{r}_i$ for atom i. We have carried out the matrix diagonalization at equal spaced time intervals along dynamical trajectories generated in the molecular dynamics simulation.

Figure 10 shows how the average number $\langle n_{pos} \rangle$ of positive eigenvalues ($\omega^2 > 0$) varies with temperature. Three eigenvalues are always zero, owing to the free translational motion of the system as a whole with periodic boundary conditions. Therefore in the low-temperature limit we expect, and indeed find, 447 positive eigenvalues as the 150-atom system executes harmonic motion near a single Φ minimum. However, the mean number of positive eigenvalues displays an immediate decline as temperature rises. Since $\omega^2 < 0$ indicates the existence of a direc-

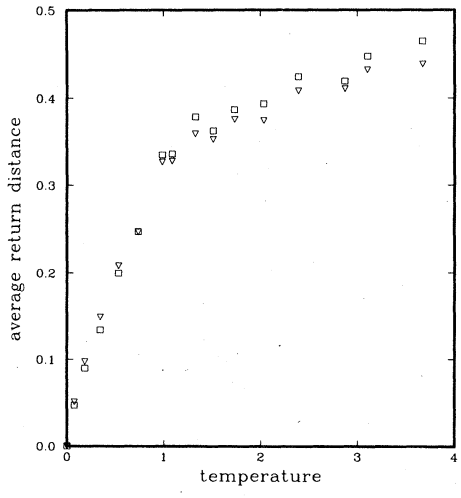

FIG. 9. Average distance the atoms move to arrive at the minimum potential energy quench configuration as a function of temperature, both in reduced units. The squares are the P atom distances and the triangles are the Ni atom distances.

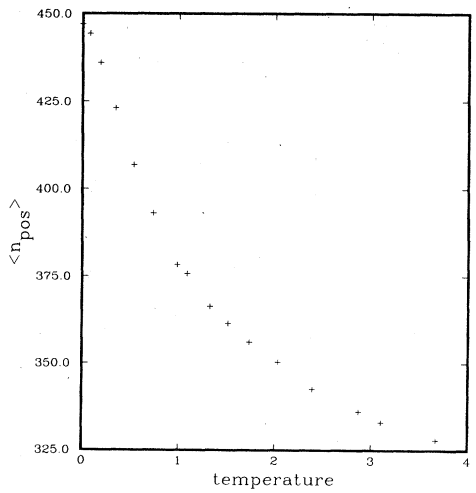

FIG. 10. Average number of positive eigenvalues of the Hessian matrix as a function of temperature in reduced units.

TABLE I. Table of transition states.

Case	Φ_{ts}	Φ_A	Φ_B	M_P	M_{Ni}
(a)	−894.500 13	−894.530 46	−894.501 28	17.730	17.358
(b)	−897.757 47	−897.811 30	−897.764 76	3.109	29.710
(c)	−897.040 25	−897.764 76	−897.141 57	9.839	6.733
(d)	−897.126 13	−898.268 79	−898.741 76	7.639	102.292
(e)	−898.552 95	−898.741 76	−898.553 75	17.600	43.903
(f)	−898.009 38	−898.047 23	−898.082 05	8.535	12.316

tion of negative curvature on the Φ hypersurface, these negative eigenvalues are an indicator of anharmonicity.

When the same matrix diagonalization is carried out for a single-component system in its crystalline phase,[19,20] the low-temperature behavior contrasts strongly with that shown in Fig. 10 for the amorphous Ni-P system. Instead of the immediate decline shown, $\langle n_{pos} \rangle$ remains substantially constant and equal to its zero-temperature limit up to a significant fraction (≈ 0.2 of the melting temperature); this is to be expected for a system confined to the deep and isolated region surrounding an absolute minimum (crystalline packing). However in an amorphous solid there always appear to exist a distributed collection of low-barrier "two-level" degrees of freedom whose anharmonicity can be elicited by minimal thermal agitation. We suggest therefore that the low-temperature limiting behavior of $\langle n_{pos} \rangle$ can be a powerful tool in determining the density and barrier distribution of these important bistable degrees of freedom.

V. FUNDAMENTAL TRANSITIONS

During the evolution of a dynamical trajectory in phase space, the system penetrates a sequence of quench regions surrounding distinct potential minima. These regions are defined to be the sets of configurations all of which connect to a common interior Φ minimum via the mass-weighted steepest-descent quench mapping [Eq. (2.8)]. At low-temperature successive mappings to quench minima will consistently fall into the same configuration until eventually the system leaves the region of that one minimum and passes into the region of another minimum. At higher temperature mean residence time in any minimum region will be shorter. Figure 11 shows the depths for minima mapped out every 0.031 36 ps for three different low-temperature dynamical trajectories. The top panel shows the quench chronology for a trajectory where eight different minimum energy configurations were found with a total of twelve transitions between regions. The characteristic signature of an active bistable ("two-level") system appears in the latter part of this sequence. It has been proposed that such bilevel oscillators are important in the low-temperature specific heat, thermal expansion, and phonon properties of amorphous solids.[14] The middle panel shows four different minimum energy configurations and a total of six transitions. The bottom panel shows five different minimum energy configurations and a total of four transitions. The arrows indicate some of the points where we have succeeded in finding the simple saddle point or "transition state" connecting the successively visited minimum regions.

The simple saddle points (as well as each minimum) are extrema of Φ satisfying

$$\Psi = (\nabla\Phi)^2 = 0 \,. \tag{5.1}$$

A simple heuristic procedure[12] has been constructed using this basic property to locate the saddle point. First two Φ minimum configurations, A and B, which are known to be connected from the dynamical trajectory mappings, are located. Then Φ is evaluated along a linear path connecting A and B. Starting at the configuration of maximal Φ along this path, the function Ψ is minimized so that Eq. (5.1) is satisfied. The Hessian matrix of second derivatives is then evaluated at the end point of the minimization and diagonalized to determine that one and only one negative eigenvalue exists to verify that indeed a simple saddle point has been found.

Starting at the simple saddle point, very small displacements (both positive and negative) along the negative-eigenvalue eigenvector direction are made followed by the usual mass-weighted steepest descent quenches to determine directly the two states which this saddle point connects. This acts as a check to ensure that we have in fact found the transition state connecting starting configurations A and B.

Six transition states have been quantitatively characterized. Table I gives their potential energies as well as those

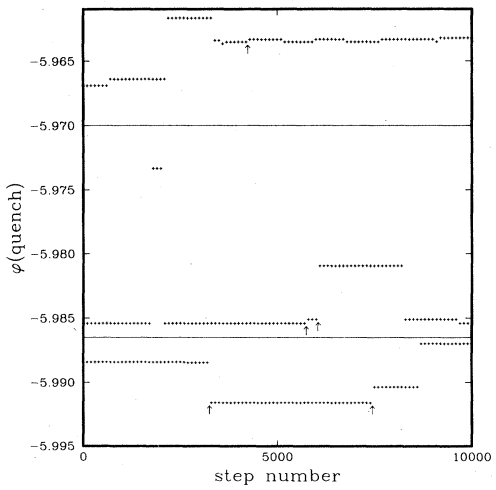

FIG. 11. Quench potential energy per atom for three different dynamical trajectories. The trajectory temperatures for the top, middle, and bottom panels were 0.2113, 0.1545, and 0.1843, respectively. The arrows indicate the points at which some of the transition states shown in Table I were determined.

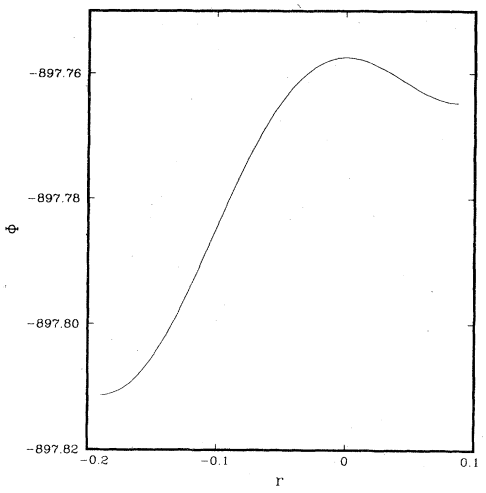

FIG. 12. Total potential energy versus distance along the reaction coordinate, both in reduced units, for transition state (b) of Table I. The transition state is located at zero. State A is on the left; state B is on the right.

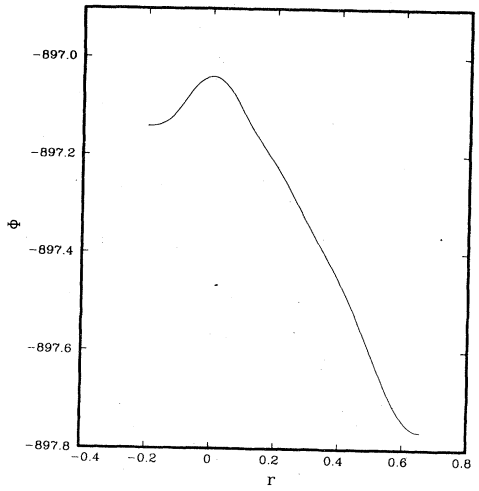

FIG. 14. Total potential energy versus distance along the reaction coordinate for transition state (c) of Table I. State B is on the left; state A is on the right.

of the flanking pairs of minima. In addition Table I shows a measure of the degree of rearrangement localization of atoms between states A and B given by

$$M_\mu = \langle \mid \mathbf{u}_i \mid^4 \rangle_\mu / \langle \mid \mathbf{u}_i \mid^2 \rangle_\mu^2 \tag{5.2a}$$

where μ = Ni,P and

$$\mathbf{u}_i = \mathbf{r}_i^{(A)} - \mathbf{r}_i^{(B)} - \mathbf{s} \ , \tag{5.2b}$$

where $\mathbf{r}_i^{(A)}$ and $\mathbf{r}_i^{(B)}$ are the coordinates of atom i in configurations A and B, respectively, and $\mathbf{s}$ is a vector which brings the centroids of A and B into coincidence. If random and nonlocal rearrangements of atoms occurred in going from state A to state B then the displacement parameters would roughly have a normal (Gaussian) distribution for which one easily calculates

$$M_\mu = \tfrac{5}{3} \ . \tag{5.3}$$

As can be seen from Table I, the M's are very large by comparison indicating that only a small number of atoms out of the entire system tend to move in going from state A to state B.

Figure 12 shows the total potential energy as a function of distance along the reaction coordinate path consisting of forward and reverse steepest-descent paths emanating from the transition state labeled (b) in the table, i.e., the transition occurring between steps 5700 and 5800 of the middle panel of Fig. 11. The path length from the transition state is defined as

$$l(R) = \int_0^R ds \left| \sum_j \frac{d\mathbf{r}_j}{ds} \right| \ , \tag{5.4}$$

where $d\mathbf{r}_j/ds$ is defined by Eq. (2.8), the mass-weighted

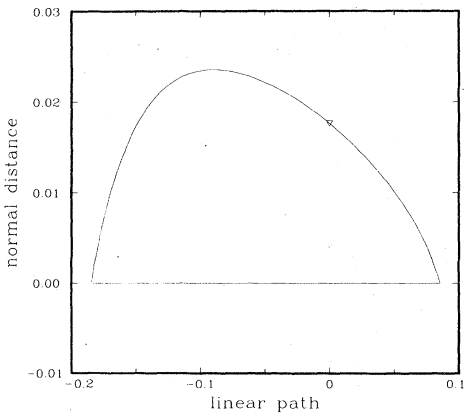

FIG. 13. Normal distance from the reaction path to the linear path connecting two states versus linear path length for transition state B of Table I. The transition-state position is indicated with a triangle. State A is on the left; state B is on the right.

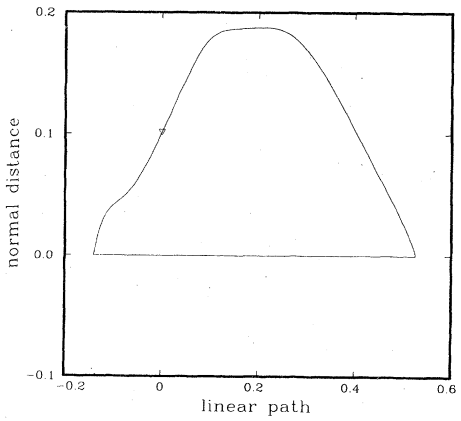

FIG. 15. Normal distance from the reaction path to the linear path connecting two states versus linear path length for transition state (c) of Table I. State B is on the left; state A is on the right.

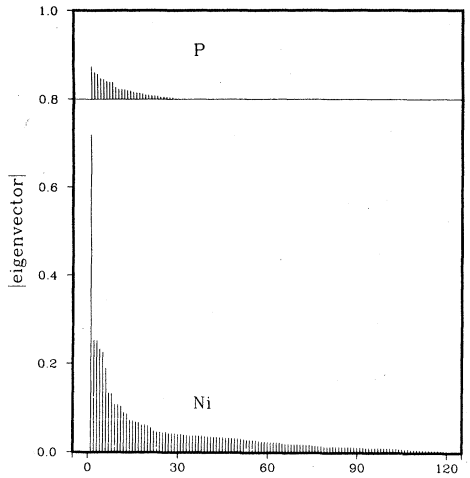

FIG. 16. Absolute values of eigenvector components for each atom of the reaction coordinate at transition state (b) of Table I. The atoms are ordered according to magnitude of the component. The P-atom components have been offset.

steepest-descent equations. The nonlinearity of the reaction coordinate is shown in Fig. 13, where the normal distance from the reaction path to the linear path connecting the two states is plotted. A triangle indicates the location of the transition state.

Figure 14 shows the total potential energy versus reaction path length for the transition state labeled (c) in Table I which occurs between steps 6000 and 6100 of the middle panel of Fig. 11. Figure 15 vividly portrays the highly nonlinear nature of the reaction coordinate path which connects the two potential minima across this transition state.

An indication of which atom or group of atoms is involved in the motion through the transition state may be obtained by looking at the components of the eigenvector of the one negative eigenvalue at the transition state.

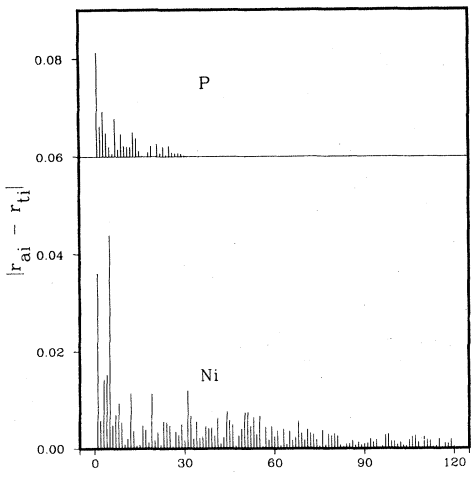

FIG. 17. Distance traversed by atoms from the transition state (b) to minimum state *A*. Each atomic distance is plotted in the order of its eigenvector component of Fig. 16.

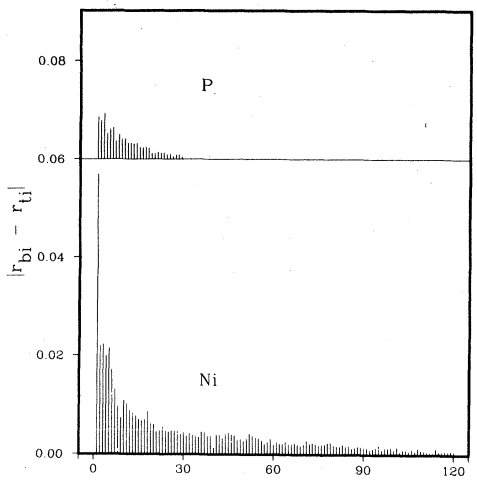

FIG. 18. Distance traversed by atoms from the transition state (b) to minimum state *B*. Same plotting order as in Fig. 17.

These components have been sorted by magnitude and atomic type, either Ni and P, and plotted in Fig. 16 for the transition state labeled (b) in Table I. The plot shows that for this case most of the motion belongs to a single Ni, with some modest participation of the surroundings, reinforcing the conclusions drawn earlier from the M_μ parameters in Table I. The distance the atoms move from the transition state to states *A* and *B* are shown in Figs. 17 and 18, respectively. The distances have been plotted in the same order as were the eigenvector components. Notice that although atoms with larger eigenvector components tend on average to move farther, the distances are not monotonically decreasing as might be expected if the transition-state geometry alone strictly governed the motion between *A* and *B*. This is particularly noticeable for the more distant minimum (Fig. 17).

Figure 19 shows an eigenvector component plot for the transition state labeled (c) in Table I. This transition state is the only one of the total of six for which a P atom has a

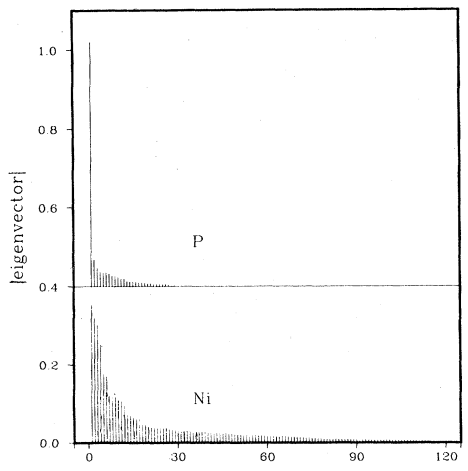

FIG. 19. Absolute values of eigenvector components for each atom of the reaction coordinate at transition state (c) of Table I.

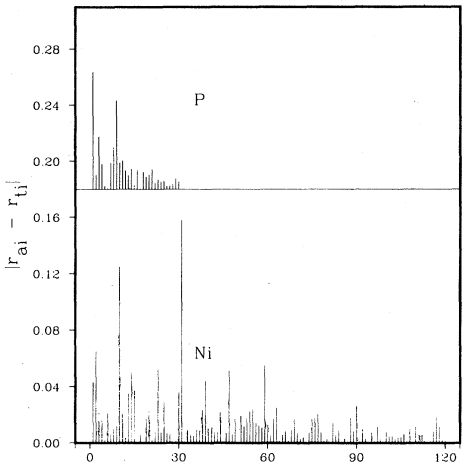

FIG. 20. Distance traversed by atoms from the transition state (c) to minimum state *A*. Each atomic distance is plotted in order of its eigenvector component of Fig. 19.

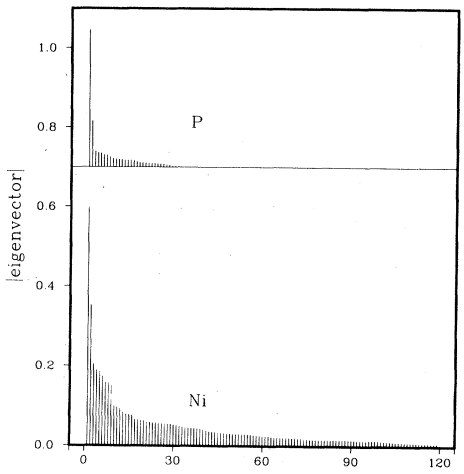

FIG. 22. Absolute values of eigenvector components for transition state (a) of Table I.

larger component than all of the Ni atoms. Figures 20 and 21 show the distances the atom must travel from the transition state to states *A* and *B*, respectively. Again the nonmonotonicity of atomic distances is most evident for the state farther from the transition state.

Two pairs of successively surmounted transition states are connected through sharing of the region surrounding a single Φ minimum. We can ask whether the successive transitions are geometrically correlated. For transition states labeled (b) and (c), we find that the inner product of their reaction coordinate eigenvectors is

$$\mathbf{e}_b \cdot \mathbf{e}_c = -0.0496 \ . \tag{5.5}$$

For transition states labeled (d) and (f) the inner product of their transition state reaction coordinate eigenvectors is

$$\mathbf{e}_d \cdot \mathbf{e}_f = 0.0129 \ . \tag{5.6}$$

These results seem to indicate (at least for the Ni-P model) that successive transitions are usually localized on rather distinct subsets of the atoms.

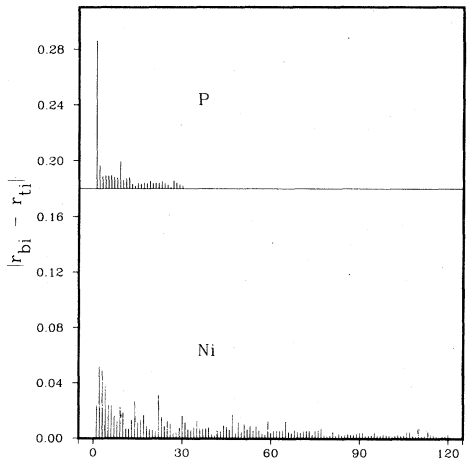

FIG. 21. Distance traversed by atoms from the transition state (c) to minimum state *B*. Same plotting order as Fig. 19.

Figures 16 and 19 show cases in which the reaction coordinate at the transition state clearly singles out a single atom to bear most of the motion. However, that is not always the case. Figure 22 presents another case [transition state (a) in Table I] for which primary atomic motions at the transition state appear to be distributed over a larger group of both Ni and P atoms.

VI. DISCUSSION

The primary objective pursued in this paper is understanding the structure and kinetics in the Ni-P alloy system from the standpoint of the multidimensional geometry of the potential-energy hypersurface. In pursuing this objective it has been necessary to map configurations occurring along the dynamical trajectory onto nearby potential minima by means of a mass-weighted steepest-descent connection. The novel insights that emerge from this approach appear to justify the extra computational effort required.

In particular, the mapping to minima ("quenching") is a potent device for enhancing the image of short-range order that is present in the pair- (and higher order) distribution functions. Consistent with earlier findings for a wide variety of model substances,[6–13] we have found that under constant density conditions this image enhancement reveals a common inherent structure that underlies the stable liquid phase, regardless of temperature. Because of the conceptual simplicity this observation brings to liquid-state theory, it is important in future modeling studies to see how well it applies to other glass-forming substances, such as B_2O_3 and Se. Also, effort should be devoted to devising analytical predictive theory of the inherent structures (random packings) themselves, as well as a theory of the fundamentally anharmonic process that reconstitutes measurable pair-correlation functions at various temperatures from the inherent structures.

Perhaps the greatest advantage offered by our multidi-

mensional geometric approach is its facility for identifying and characterizing the low-barrier bistable degrees of freedom that dominate properties of many amorphous materials at low temperature. The transition states and associated reaction pathways reported in Sec. V show that the bistable degrees of freedom are localized but cooperative. Furthermore they are diverse in nature, with considerable variation in barrier height, asymmetry, number and types of atoms involved, and extent of curvature of the reaction pathway. Attempts to identify bistable degrees of freedom by separately testing motion of individual atoms[21] will almost certainly produce misleading results. In our opinion, more simulation of the type advocated herein is justified to understand low-temperature amorphous substances in greater qualitative and quantitative detail.

[1]*Amorphous Semiconductor Technologies and Devices,* edited by Y. Hamakawa (North-Holland, New York, 1982).
[2]J. G. Mohr and W. P. Rowe, *Fiber Glass* (Van Nostrand/Reinhold, New York, 1978).
[3]J. Mort and I. Chen, in *Applied Solid State Science,* edited by R. Wolfe (Academic, New York, 1975), Vol. 5, pp. 69—149.
[4]*Structure and Mobility in Molecular and Atomic Glass,* edited by J. M. O'Reilly and M. Goldstein [Ann. N.Y. Acad. Sci. **371**, 1 (1981)].
[5]T. A. Weber and F. H. Stillinger, Phys. Rev. B **31**, 1954 (1985).
[6]F. H. Stillinger and T. A. Weber, Phys. Rev. A **28**, 2408 (1983).
[7]F. H. Stillinger and T. A. Weber, J. Phys. Chem. **87**, 2833 (1983).
[8]T. A. Weber and F. H. Stillinger, J. Chem. Phys. **80**, 2742 (1984).
[9]F. H. Stillinger and T. A. Weber, J. Chem. Phys. **80**, 4434 (1984).
[10]F. H. Stillinger and T. A. Weber, Science **225**, 983 (1984).
[11]T. A. Weber and F. H. Stillinger, J. Chem. Phys. **81**, 5089 (1984).
[12]F. H. Stillinger and T. A. Weber, J. Chem. Phys. **81**, 5095 (1984).
[13]F. H. Stillinger and T. A. Weber, Phys. Rev. B **31**, 5262 (1985).
[14]P. W. Anderson, B. I. Halperin, and C. M. Varma, Philos. Mag. **25**, 1 (1972).
[15]*Amorphous Solids: Low-Temperature Properties,* edited by W. A. Phillips (Springer, Berlin, 1981).
[16]G. S. Cargill III, J. Appl. Phys. **41**, 12 (1970).
[17]C. W. Gear, Argonne National Laboratory Report No. ANL-7126, January, 1966 (unpublished).
[18]R. Fletcher, *Practical Methods of Optimization* (Wiley, New York, 1980).
[19]R. A. LaViolette and F. H. Stillinger, J. Chem. Phys. (to be published).
[20]F. H. Stillinger and T. A. Weber, J. Chem. Phys. (to be published).
[21]R. Harris and L. J. Lewis, Phys. Rev. B **25**, 4997 (1982).